DSC study of the interaction of the prion peptide PrP106–126 with artificial membranes

D. Grasso,*[a] D. Milardi,[a] C. La Rosa[a] and E. Rizzarelli[a,b]

[a] *Dipartimento di Scienze Chimiche, Universita' di Catania, Viale Andrea Doria 6, 95125 Catania, Italy. E-mail: dgrasso@dipchi.unict.it*

[b] *Istituto CNR per lo Studio delle Sostanze Naturali di Interesse Alimentare e Chimico Farmaceutico, Sezione per lo Studio di Modelli di Metallo Enzimi, Viale Andrea Doria 6, 95125 Catania, Italy*

Received (in London, UK) 11th July 2001, Accepted 17th September 2001
First published as an Advance Article on the web

The incorporation of the human prion peptide PrP106–126 into 1,2-dipalmitoyl-sn-glycero-3-phosphocholine (DPPC) and 1,2-dipalmitoyl-sn-glycero-3-phosphoethanolamine (DPPE) host model membranes has been investigated by differential scanning calorimetry. Two different types of peptide–membrane interactions have been studied. In one case, the peptide is obliged to be included into the hydrocarbon region of the lipid bilayer, in the other case, it is allowed to interact with the external surface of the membrane. The PrP106–126 incorporated into the DPPC membrane shows an increase in the gel–liquid crystal transition temperature of the bilayer with a decreased enthalpy change. The "oriented" insertion of the hydrophobic part of the fragment into the bilayer, with a consequent increase in the order of the lipidic hydrocarbon chains in the gel state, is responsible for this behavior. Independently from the procedure adopted for the preparation of the sample, the PrP106–126 fragment interacts strongly and irreversibly with the host membrane. In contrast, when PrP106–126 is incorporated in the DPPE model membrane, the gel–liquid crystal transition temperature of the bilayer and the associated enthalpy change decrease. When added externally to the DPPE model membrane, the PrP106–126 fragment has no effect on the phase behavior of the bilayer. These findings suggest that PrP106–126 has a specific affinity for DPPC membranes that might correspond to the external surface of cells.

Introduction

Prion diseases such as scrapie in sheep and goats, bovine spongiform encephalopathy, Creutzfeldt–Jakob disease (CJD) and Gerstmann–Straussler–Scheinker disease (GSS) in humans are characterized by the accumulation of abnormal forms of the cellular prion protein (PrP^c), termed $PrPr^{sc}$, in the brain.[1] In contrast with PrP^c, $PrPr^{sc}$ is partly resistant to digestion with protease and has a marked tendency to form insoluble aggregates and amyloid fibrils.[2–4] The accumulation of PrP^{sc} as amyloid in the brain is thought to be responsible for the nerve cell degeneration, astrogliosis and activation of microglial cells observed in prion-related encephalopathies.[5–7]

Recent NMR studies of PrP^c indicate that the normal protein is composed of two structurally distinct moieties: an extended N-terminal segment (residues 23–125) with features of a flexibly disordered polypeptide chain containing four octarepeat sequences (residues 60–91), and a well-defined globular domain (residues 126–231) with three α-helices and a two-stranded anti-parallel β-sheet.[8–10] The $PrP^c \rightarrow PrP^{sc}$ conversion features a conformational change with a decrease in the α-helical secondary structure and a striking increase in the β-sheet content.[11–13]

The mechanism by which PrP^{sc} causes infectivity and neurodegeneration is still unknown; however, there are indications that cellular plasma membranes are important in the disease process. In particular, PrP^{sc} has been shown to (i) increase membrane microviscosity (ii) result in abnormal receptor-mediated calcium ion responses, and (iii) lead to membrane protein alterations.[14–16] The identification of the minimal segment involved in amyloid formation[17] and the evidence that the cleavage of the N-terminus (residues 23–88) and the deletion of residues 141–176 do not obstruct the formation of PrP^{sc},[18,19] suggested that, at least for some cases, the protein part containing the residues 90–140 might play a central role in the conformational change of the prion protein. This hypothesis prompted a number of studies concerning the toxicity of prion peptide fragments.[20]

In particular, previous studies have shown that a synthetic peptide with residues 106–126 of human PrP (PrP106–126) exhibits some of the pathogenic and physicochemical properties of $PrPr^{sc}$.[21,22] Even if they are still the object of some controversy,[23–25] these data indicate that the PrP region including residues 106–126 might be a suitable model for the investigation of the pathogenic mechanism of $PrPr^{sc}$, and in particular for the study of the peptide-induced perturbation of the cell membrane.

In general, the thermotropic phase behavior of lipid membrane systems is highly affected by the presence of guest molecules such as peptides. In particular, the effect on the thermally-induced gel–liquid crystal phase transition and the related thermodynamic variables (melting temperature, T_m, enthalpy change, ΔH, and entropy change, ΔS) depends on the nature of the interactions between these two classes of biological membrane constituents and on the general topology of the peptide relative to the lipid bilayer.[26] The most powerful technique for such studies is probably differential scanning calorimetry (DSC), a convenient and sensitive thermal method which provides reliable thermodynamic information on the effects of peptides on the thermotropic phase behavior of the host lipid bilayer.[27]

To the best of our knowledge, no DSC data concerning the interaction of the PrP106–126 peptide with lipid membranes are available in literature. In this work, DSC has been extensively used to study the interactions of the prion peptide fragment PrP106–126 with DPPC and DPPE model membranes which are mainly located at the exterior and interior of the cell, respectively.[28]

In order to correctly interpret our results, we have initially studied the calorimetric effect on the thermally-induced gel–liquid crystal phase transition of systems where a series of small hydrophobic peptides (Phe-Gly, Phe-Gly-Gly and Phe-Gly-Phe-Gly) are dissolved into DPPC model membranes. The different calorimetric behavior of DPPC/PrP106–126 and DPPE/PrP106–126 systems has been also investigated comparatively *versus* different preparation protocols for the peptide–lipid complex.

The whole of the results indicate that the prion fragment PrP106–126, has a remarkable affinity with the DPPC membrane bilayer. This interaction is independent from the preparation procedure used for the samples, from the physical state of the bilayer and from kinetic factors. These findings are explained in terms of the topology of the peptide–lipid complexes.

On the other hand, PrP106–126, if incorporated into the bilayer, has a destabilizing effect on the thermotropic phase behavior of the DPPE membrane or, alternatively, no effect when it interacts with the exterior of this membrane.

Materials and methods

Chemicals

The peptide PrP106–126 (Lys-Thr-Asn-Met-Lys-His-Met-Ala-Gly-Ala-Ala-Ala-Ala-Gly-Ala-Val-Val-Gly-Gly-Leu-Gly), and small peptides Phe-Gly, Phe-Gly-Gly, Phe-Gly-Phe-Gly, were obtained from Bachem. 1,2-dipalmitoyl-sn-glycero-3-phosphocholine (DPPC) and 1,2 -dipalmitoyl-sn-glycero-3-phosphoethanolamine (DPPE) were obtained from Fluka. All inorganic salts for phosphate buffer preparation were purchased from Sigma Chemical Co.

Preparation of pure multilamellar vesicles (MLV)

Model membranes were prepared as described elsewhere.[29] Briefly, solutions of pure phospholipids in $CHCl_3$ were dried under nitrogen and evaporated under high vacuum to dryness in round-bottomed flasks. The resulting lipid film on the wall of the flask was hydrated with an appropriate volume of 10 mM phosphate buffer (pH 7.0 and 0.1 M ionic strength in NaCl) and dispersed by vigorous stirring in a water bath set at 4 °C above the gel–liquid crystal transition temperature of the membrane. The final nominal concentration of the lipid was 2 mg ml^{-1}.

Preparation of pure large unilamellar vesicles (LUV)

The multilamellar vesicles were extruded through polycarbonate filters (pore size = 100 nm) (Nuclepore, Pleasanton, CA) mounted in a mini-extruder (Avestin Inc.) fitted with two 0.5 ml Hamilton gas-tight syringes (Hamilton, Reno, NV). Usually, we subjected samples to 19 passes through two filters in tandem as recommended elsewhere.[30] An odd number of passages was performed to avoid contamination of the sample by vesicles which might not have passed through the filter.

Incorporation of peptide fragments in model membranes

Three different protocols have been applied to prepare mixed lipid–peptide bilayers: (A) the peptide fragment was dissolved in the same organic solution ($CHCl_3$) as the phospholipid (molar ratio peptide : lipid of 1 : 10). The peptide–lipid organic solution was dried under nitrogen and evaporated under high vacuum to dryness in round-bottomed flasks. The MLV membrane was then obtained as described above; (B) the MLV–peptide model membranes were extruded as previously described to prepare large unilamellar vesicles; (C) an appropriate amount of peptide was added to previously prepared membrane suspensions to give a final peptide : lipid molar ratio of 1 : 10. The mixture was initially vigorously vortexed for 1–2 min and, unless otherwise specified, immediately scanned.

Differential scanning calorimetry

DSC scans were carried out with a second generation high-sensitivity SETARAM micro differential scanning calorimeter (microDSC II) with 1 ml stainless steel sample cells, interfaced with a BULL 200 Micral computer. The sampling rate was 1 $point^{-1}$ in all measuring ranges. The same solution without the sample was used in the reference cell. Both the sample and reference were heated with a precision of 0.05 °C at a scanning rate of 0.5 °C min^{-1}. In order to obtain the excess heat capacity (C_{exc}) curves; buffer–buffer baselines were recorded at the same scanning rate and then subtracted from the sample scans as previously described.[19] The average level of noise was about $\pm$ 0.4 μW and the reproducibility at refilling was about 0.1 mJ K^{-1} ml^{-1}. Calibration in energy was obtained by using a definite power supply, electrically generated by an EJ2 SETARAM Joule calibrator within the sample cell. To check the reproducibility of the results, three different samples were scanned. For each sample, three heating and two cooling scans were recorded. Cooling scans yielded curves very similar to the heating scans, but, in accord with the literature,[31] the transitions in the cooling curves are shifted, by about 1 °C, to lower temperatures. Therefore, due to the supercooling phenomenon, accurate thermotropic transitions are evaluated from heating curves. For this reason, only heating scans are discussed in this work. In the case of DPPC model membranes, only the main transition is considered because the pre-transition is strongly dependent on the preparative method used to obtain the membrane and it disappears when the liposomes are extruded.[33]

Results and discussion

The complexity of the thermodynamic principles underlying the binding of peptides and proteins to lipid bilayers has, till now, prevented a detailed understanding of biomolecular membrane association phenomena. Major contributions to the overall change in the free energy upon peptide binding are expected to arise from electrostatic interactions and hydrophobic effects. The latter force is responsible for driving the penetration of hydrophobic peptides into the core of the membrane. As a consequence of this insertion, the bilayer undergoes lipid rearrangements according to the chemical and structural features of the peptide.

The use of small hydrophobic peptides of different length can be helpful in elucidating how the different chemistry of the perturbing peptide can affect the DSC curves of the host membrane.

DSC of small peptides–bilayer systems

The C_{exc} profiles of pure DPPC MLV bilayers and of different peptide–lipid systems are showed in Fig. 1 and the corresponding thermodynamic parameters reported in Table 1. Scans of the MLVs of pure DPPC show the DSC peak corresponding to the gel–liquid crystal phase transition located at

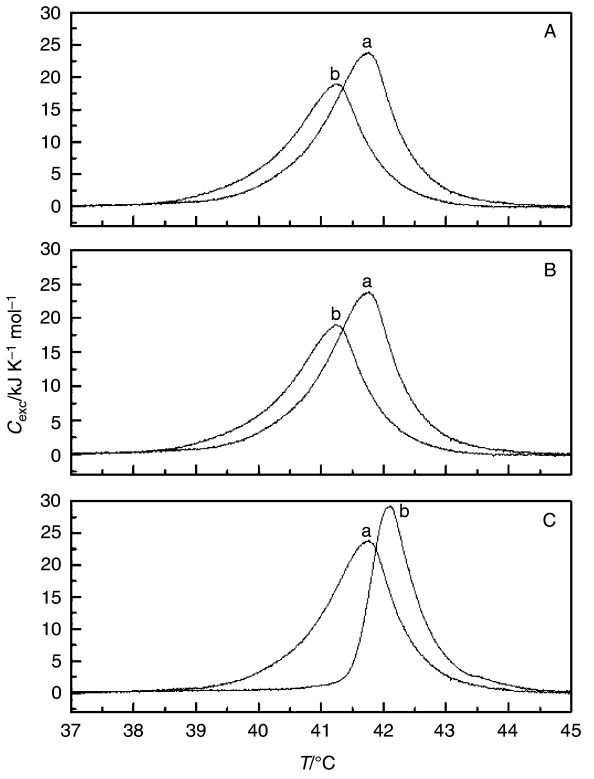

Fig. 1 DSC curves for mixtures of DPPC multi lamellar vesicles and small peptides prepared according to method A. The DSC curves relating to DPPC/Phe-Gly, DPPC/Phe-Gly-Gly and DPPC/Phe-Gly-Phe-Gly systems are reported in (A B and C), respectively. Curves a and b represent the DSC transitions of a pure DPPC MLV membrane and of the lipid–peptide systems, respectively. The heating rate was 0.5 K min^{-1}. All the samples were prepared in 10 mM phosphate buffer pH = 7.0, ionic strength was adjusted to 0.1 M with sodium chloride.

Table 1 Calorimetric peak temperatures (T_m), total enthalpy changes (ΔH) and width of the peak at half height (W) relative to the different peptide–lipid bilayer systems. The preparation of each different system and the experimental conditions adopted are described in Materials and methods. Experimental values are reported as the mean ± the standard deviation of three repeated experiments.

	T_m/°C	ΔH /kJ mol^{-1}	W/°C
DPPC MLV	41.7 ± 0.05	38.3 ± 1.1	1.51 ± 0.03
DPPC LUV	41.6 ± 0.06	36.0 ± 0.7	1.19 ± 0.02
DPPE MLV	62.4 ± 0.05	36.0 ± 1.1	1.21 ± 0.05
DPPE LUV	62.6 ± 0.06	32.5 ± 1.0	1.30 ± 0.03
DPPC MLV/FG	41.2 ± 0.07	31.5 ± 1.1	1.63 ± 0.02
DPPC MLV/FGG	41.2 ± 0.05	36.7 ± 1.0	1.63 ± 0.03
DPPC MLV/FGFG	42.1 ± 0.06	31.0 ± 0.8	0.90 ± 0.01
DPPC MLV/PrP106–126	42.0 ± 0.07	26.5 ± 0.8	0.96 ± 0.04
DPPC LUV/PrP106–126	42.3 ± 0.05	26.5 ± 0.9	1.16 ± 0.05
DPPC LUV + PrP106–126	42.1 ± 0.07	26.5 ± 1.0	1.15 ± 0.03
DPPE MLV/PrP106–126	61.4 ± 0.07	15.5 ± 0.9	1.34 ± 0.02
DPPE LUV/PrP106–126	61.0 ± 0.08	10.8 ± 0.8	1.71 ± 0.04
DPPE LUV + PrP106–126	62.6 ± 0.07	32.5 ± 0.8	1.30 ± 0.04

$T_m = 41.7$ °C, in agreement with previous reports.[33] It is evident from Fig. 1 how the thermal transition of DPPC is differently affected by the presence of the peptides in the membrane. In particular, Phe-Gly and Phe-Gly-Gly shifted (by about 0.5 °C) the DSC peak to lower temperatures and the associated enthalpy change decreased by about 18 and 4%, respectively [Fig. 1 (A and B)]. The shapes of the DSC curves for both systems are not changed, as evidenced by the peak width at half height values ($W = 1.63$ °C) reported in Table 1.

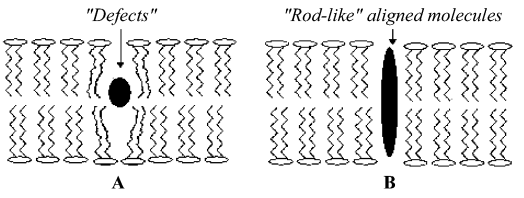

Fig. 2 Schematic drawings of the possible interactions of the guest peptide with a host lipid bilayer.

On the other hand, as the peptide length is increased by one hydrophobic unit (Phe-Gly-Phe-Gly) the effect is noticeably different [Fig. 1 (C)]. In fact the transition temperature of the system increases by about 0.5 °C with respect to the pure DPPC MLV bilayer, the corresponding ΔH is decreased by about 7 kJ mol^{-1} (19%) and the DSC curve is sharpened ($W = 0.90$).

This behaviour can be qualitatively explained if we consider that a guest peptide can interact with the host membrane according to two different mechanisms (A and B), schematically represented in Fig. 2.

In the first case, the peptide acts as a "defect" in the membrane bilayer, being randomly dispersed in the hydrocarbon region with a consequent increase in the disorder of the surrounding lipids when the system is below the gel–liquid crystal transition temperature. In this case, the electrostatic charges and the geometric features of the guest molecule perturb the lipid–lipid interactions, giving rise to a decrease in the rigidity and stability of the membrane. The DSC peak relative to such a peptide–membrane system, if compared with the behaviour of a pure membrane, should exhibit lower T_m, ΔH and sharpness, which is believed to be related to the rigidity of the membrane. This model is consistent with the thermal behaviour of the DPPC MLV/FG system.

In the second case, the rod-like geometry and hydrophobicity of the guest peptide allows it to fit into the membrane aligned parallel to the direction of the bilayer. In this case, lipid–peptide hydrophobic forces act cooperatively to increase the local order and the rigidity of the membrane; as a consequence, T_m is expected to increase and W to decrease (increased sharpness of the peak). On the other hand, because of the hydrophobic interactions, the lipid molecules surrounding the peptide are "blocked" and are not subject to the transition as the temperature increases. In such a system, the total energy involved in the transition (ΔH) is decreased with respect to the pure DPPC because the number of lipid molecules involved in the temperature-induced transition is decreased. This model is consistent with the thermal behaviour of the DPPC MLV/FGFG system. This behavior has been previously observed for other hydrophobic bioactive peptides.[34] The DPPC MLV/FGG system is an intermediate situation in which the two mechanisms are convoluted.

DSC of DPPC/PrP106–126 systems

Fig. 3(A) shows the C_{exc} profile of MLVs of pure DPPC (curve a) and of DPPC/PrP106–126 (curve b) systems. The thermally-induced transition appears remarkably affected by the presence of PrP106–126 in the membrane, being sharpened (W changes from 1.51 to 0.96 °C) and shifted to higher temperatures (T_m is increased by 0.3 °C). In contrast, the transition enthalpy decreases from 38.3 to 26.5 kJ mol^{-1}, as reported in Table 1. Analogous behavior was observed for LUV systems, as evidenced by Fig. 3(B). In particular, the presence of PrP106–126 in DPPE LUV membranes induces an increase of T_m (from 41.6 to 42.3 °C), a decrease of ΔH (from 36.0 to 26.5 kJ mol^{-1}) and a small decrease of W (from 1.19 to 1.16). It should be noted that the effects of the incorporation of PrP106–126 into the DPPC

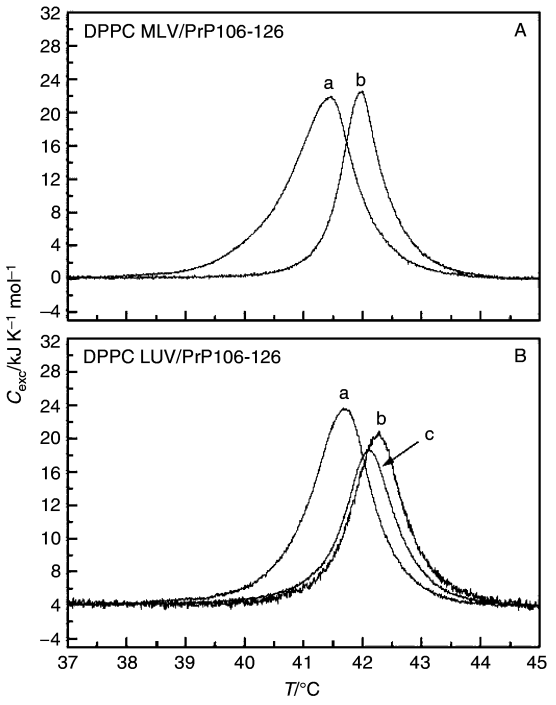

Fig. 3 (A) DSC curves for mixtures of PrP106–126/DPPC (peptide : lipid molar ratio 1 : 10) multi lamellar vesicles prepared according to method A (curve b). (B) DSC curves for mixtures of PrP106–126/DPPC (peptide : lipid molar ratio 1 : 10) large unilamellar vesicles prepared according to methods B (curve b) and C (curve c). Curves labelled a represent the DSC transition of a pure DPPC MLV model membrane. The heating rate was 0.5 K min^{-1}. All the samples were prepared in 10 mM phosphate buffer pH = 7.0, ionic strength was adjusted to 0.1 M with sodium chloride.

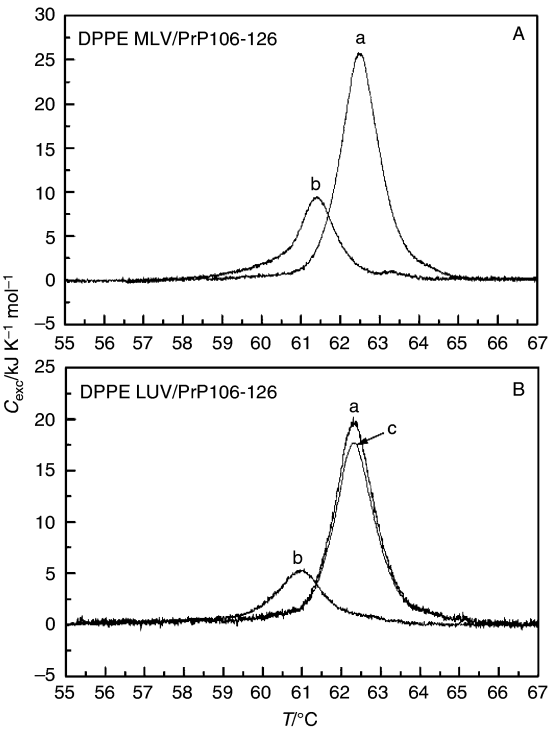

Fig. 4 (A) DSC curves for mixtures of PrP106–126/DPPE (peptide : lipid molar ratio 1 : 10) multi lamellar vesicles prepared according to method A (curve b). (B) DSC curves for mixtures of PrP106–126/DPPE (peptide : lipid molar ratio 1 : 10) large unilamellar vesicles prepared according to methods B (curve b) and C (curve c). Curves labelled a represent the DSC transition of a pure DPPE MLV model membrane. The heating rate was 0.5 K min^{-1}. All the samples were prepared in 10 mM phosphate buffer pH = 7.0, ionic strength was adjusted to 0.1 M with sodium chloride.

bilayer show a similarity with the behaviour of the DPPC MLV/FGFG system, thus suggesting that this fragment interacts with DPPC membranes according to model B represented in Fig. 2. In Fig. 3(B), curve c represents the C_{exc} profile of LUV bilayers suspended with PrP106–126 prepared according to method C (see DPPC LUV + PrP106–126 in Table) reported in the Experimental: the DSC curve is very similar to that corresponding to the membrane in which the prion fragment was directly incorporated into the bilayer [Fig. 3(B) curve b]. Several DSC scans of this system, recorded at different times of incubation (up to 24 h) either at room temperature or at 4 °C above the transition temperature, did not differ from the previous one, testifying to the absence of any kinetic factor in this kind of interaction and the independence of the lipid–peptide interaction from the physical state (gel or liquid crystal) of the membrane.

DSC of DPPE/PrP106–126 system

Fig. 4(A) shows the C_{exc} profiles of MLVs of pure DPPE (curve a) and of DPPE/PrP106–126 (curve b) systems. The phase transition appears remarkably affected by the presence of PrP106–126 in the membrane, being shifted to lower temperatures (T_m decreases by 1 °C). The transition enthalpy decreases from 36.0 to 15.5 kJ mol^{-1} (see Table 1) and the curve is broadened (W changes from 1.21 to 1.34 °C). In the same curve, a very small shoulder located at about 63.3 °C can be seen, but its nature is unknown. Analogous behaviour was observed for LUV systems, as shown in Fig. 4(B). In particular, the presence of PrP106–126 in the DPPE LUV membrane induces a decrease of T_m from 62.6 to 61.0 °C, a decrease of ΔH from 32.5 to 10.8 kJ mol^{-1} and an increase of W from 1.30 to 1.71 °C. It should be noted that the effects of the incorporation of PrP106–126 into the DPPE membranes show a similarity with the behaviour of the DPPC MLV/FG system, thus suggesting that this fragment interacts with DPPE membranes according to model A in Fig. 2.

In Fig. 4(B), curve c represents the C_{exc} profile of DPPE LUV bilayers suspended with PrP106–126 prepared according to method C reported in the Experimental. The corresponding DSC curve is very similar to that corresponding to the pure membrane. Several DSC scans of this system, recorded at different times of incubation (up to 24 h) either at room temperature or at 4 °C above the gel–liquid crystal transition temperature, did not differ from the previous one, testifying to the absence of any kinetic factor and the independence of the interaction from the physical state of the membrane.

For DPPE/PrP106–126 systems, these effects of peptide incorporation into the membrane are dependent on the preparative method used to obtain the sample. In fact, from data reported in Table 1, it can be seen that the destabilizing effect of the peptide is much more evident in samples prepared according to method B (DPPE LUV/PrP106–126); on the other hand, samples prepared according to method C (DPPE LUV + PrP106–126) show thermal behaviour very similar to that of the pure membrane. This can be explained by considering the different nature of the polar heads of DPPE, which that are more hydrophilic with respect to DPPC. The effect of the incorporation of the peptide into DPPE is amplified by the extrusion process, probably ascribable to a decrease in vesicle size due to the presence of the peptide. When the peptide interacts with the external surface of the DPPE membrane (DPPE LUV + PrP106–126 systems) the polar heads create an effective shield which hampers the interaction of the bilayer with the fragment. All these findings can have important consequences in the understanding of the mechanism of interaction of PrP106–126 with the cell.

Abnormalities in plasma membrane properties[35] and ion channel functions of neurons[36] have been suggested to play a key role in the pathogenesis of prion diseases. Unlike other PrP peptides, PrP106–126 has two distinct hydrophilic and hydrophobic moieties which mimic the transmembrane domain of proteins.[37,38] Thus, the previously observed increase in membrane microviscosity and rigidification caused by this peptide might depend on its capacity to enter the cell membrane.[39]

However, the natural cell membrane is too complex a system for a detailed molecular *in vitro* approach to the investigation of the (PrP106–126)–membrane interaction and thus proper simplified model membranes are required. In natural membranes, sugars, proteins and cholesterol are immersed in a phospholipid matrix with an asymmetric composition: choline, the most abundant lipid component of outer side of the cell membrane, contains one or more unsaturated fatty acids that maintain the natural cell bilayer in the fluid liquid crystalline state at room temperature.[40] For this reason, the natural cell membrane is difficult to study by physico-chemical approaches. T hus, model systems have to be chosen in order to allow thermotropic behavior which, in turn, can give a wealth of information concerning the modifications induced in the bilayer by a guest molecule.

In this contribution, we have selected model membrane systems either with a choline or ethanolamine polar head in order to simulate the interaction of the prion fragment with the lumen and the cytosol of the cell, respectively. Moreover, in the phospholipidic matrix adopted, only saturated hydrocarbon chains are present, allowing the membrane to perform a perfectly defined gel–liquid crystalline phase transition which can give information on the interaction between the membrane and host molecules.

Our DSC results show that the PrP106–126 prion fragment has a remarkable effect on the cooperativity and on the thermodynamic properties of MLVs and LUVs of DPPC. The most interesting results are the changes in the thermotropic effects on LUV bilayers when the prion fragment is dissolved in the buffer solution, thereby interacting with the external surface of the model membrane. The corresponding transition peak is similar to that obtained when the prion fragment and lipid were dissolved together in the organic phase. Moreover, when DPPC MLV/PrP106–126 systems are extruded, in the obtained LUV/PrP106–126 sample, no significant changes were observed in the corresponding C_{exc} profile. This means that the PrP106–126 prion fragment interacts strongly and irreversibly with the DPPC bilayer. Moreover, this interaction is very rapid, as evidenced by the absence of any kinetic factor. This is a result of the hydrophobic character of the investigated fragment. In addition, it is noteworthy that the PrP106–126 sequence is amphiphile–like. Thus, it is reasonable to suggest that the hydrophobic part is able to insert into the hydrocarbon region of the bilayer, while the hydrophilic region is oriented towards the water phase.

With reference to the interaction of PrP106–126 with DPPE model membranes, it should be noted that when the peptide is added from the external region into the lipid bilayer, no effects on the phase behavior are detected. But when the peptide is incorporated into the lipid matrix, it has a destabilizing effect, as shown by the decrease in the transition temperature and enthalpy. This suggests that PrP106–126 interacts with the cell membrane *via* a delicate balance of hydrophobic and hydrophilic forces modulated by the lipid composition (DPPC or DPPE). In fact, it adheres to the cell surface *via* the choline heads (which have more hydrophobic character compared to the ethanolamine ones), then penetrates into the hydrocarbon chains driven by hydrophobic forces. The low affinity of the PrP106–126 for the ethanolamine heads should prevent the crossing of the fragment into the cytosol, suggesting a possible accumulation mechanism for PrP106–126 in the lipid matrix of the cell. Previous studies of the role played by the PrP106–126 structure in the peptide–membrane interactions[22] have shown that an increase in the β-sheet content of the peptide increased its amyloidogenicity, its neurotoxicity and its affinity for DPPC model membranes. In turn, the presence of lipids is suggested to increase the β-sheet content of the peptide.[41] In this light, the physico-chemical approach to the study of peptide-induced modifications of the membrane proposed here could open up new scenarios in the molecular approach to the investigation of prion peptide–membrane systems. Experiments aimed at contributing to the resolution of these points are now in progress in our laboratory.

Acknowledgements

This work was partially supported by the Ministero dell'Università e della Ricerca Scientifica e Tecnologica (MURST) (grants MM03194891 and 9903032282) and the Università degli Studi di Catania. Thanks are due to Salvatore Petrantoni for his assistance with sample preparation.

References

1 S. B. Prusiner, *Science*, 1991, **252**, 1515.
2 D. C. Bolton, M. P. McKinley and S. B. Prusiner, *Science*, 1982, **218**, 1309.
3 M. P. McKinley, D. C. Bolton and S. B. Prusiner, *Cell*, 1983, **35**, 57.
4 S. J. De Armond, M. P. McKinley, R. A. Barry, M. B. Braunfeld, J. R. McColloch and S. B. Prusiner, *Cell*, 1985, **41**, 221.
5 G. Forloni, N. Angeretti, R. Chiesa, E. Monzani, M. Salmona, O. Bugiani and F. Tagliavini, *Nature*, 1993, **362**, 543.
6 G. Forloni, R. del Bo, N. Angeretti, R. Chiesa, S. Smiroldo, R. Doni, E. Ghibaudi, M. Salmona, M. Porro and L. Verga, *Eur. J. Neurosci.*, 1994, **6**, 1415.
7 D. R. Brown, B. Schmidt and H. A. Kretzschmar, *Nature*, 1996, **380**, 345.
8 R. Riek, S. Hornemann, G. Wilder, M. Billeter, R. Glockshuber and K. Wuthrich, *Nature*, 1996, **382**, 180.
9 R. Riek, S. Hornemann, G. Wilder, R. Glockshuber, and K. Wuthrich, *FEBS Lett.*, 1997, **413**, 282.
10 D. G. Donne, J. H. Viles, D. Groth, I. Mehlhorn, T. L. James, F. E. Cohen, S. B. Prusiner, P. E. Wright and H. J. Dyson, *Proc. Natl. Acad. Sci. U. S. A.*, 1997, **94**, 13 452.
11 B. W. Caughey, A. Dong, K. S. Bhat, D. Trust and W. S. Caughey, *Biochemistry*, 1991, **30**, 7672.
12 K. M. Pan, M. A. Baldwin, J. T. Nguyen, M. Gasset, A. Serban, D. Groth, I. Mehlhorn, Z. Huang, R. J. Fletterick, F. E. Cohen and S. B. Prusiner, *Proc. Natl. Acad. Sci. U. S. A.*, 1993, **90**, 10 962.
13 J. Safar, P. P. Roller, D. C. Gajdusek and C. J. Gibbs Jr, *J. Biol. Chem.*, 1993, **268**, 20 276.
14 J. Viret, D. Dormont, D. Molle, L. Court, F. Leterrier, F. Cathala, C. J. Gibbs Jr and D. C. Gajdusek, *Biochem. Biophys. Res. Commun.*, 1981, **101**, 830.
15 K. Kristensson, B. Feurstein, A. Taraboulos, W. C. Hyun, S. B. Prusiner and S. J. De Armond, *Neurology*, 1993, **43**, 2335.
16 K. Wong, Y. Qiu, W. Hyun, R. Nixon, J. Vancleef, J. Sanchez-Salazar, S. B. Prusiner and S. J. De Armond, *Neurology*, 1996, **47**, 741.
17 G. Giaccone, L. Verga, O. Bugiani, B. Frangione, D. Serban, S. B. Prusiner, M. R. Forlow, B. Ghetti and F. Tagliavini, *Proc. Natl. Acad. Sci. U. S. A.*, 1992, **89**, 9349.
18 T. Muramoto, M. Scott, F. E. Cohen and S. B. Prusiner, *Proc. Natl. Acad. Sci. U. S. A.*, 1996, **93**, 15 457.
19 S. Supattapone, P. Bousque, T. Muramoto, H. Wille, C. Aagaard, D. Peretz, H. O. Nguyen, C. Heinrich, M. Torchia, J. Safar, F. E. Cohen, S. J. De Armond, S. B. Prusiner and M. Scott, *Cell*, 1999, **96**, 869.
20 C. Holscher, H. Delius and A. Burkle, *J. Virol.*, 1998, **72**, 1153.
21 D. R. Brown, J. Herms and H. A. Kretzschmar, *Neurology*, 1994, **5**, 2057.
22 M. J. Jobling, L. R. Stewart, A. R. White, C. McLean, A. Friedhuber, F. Maher, K. Beyreuter, C. L. Masters, C. Barrow, S. J. Collins and R. Cappai, *J. Neurochem.*, 1999, **73**, 1557.
23 B. Kuntz, E. Sandmeyer and P. Christen, *FEBS Lett.*, 1999, **485**, 65.
24 D. R. Brown, *FEBS Lett.*, 1999, **460**, 559.

25 G. Forloni, M. Salmona, O. Bugiani and F. Tagliavini, *FEBS Lett*., 2000, **466**, 205.
26 D. Chapman (ed.), in *Biological Membranes*, Academic Press, New York, 1982 vol. 4, p. 179.
27 K. Lohner and E. J. Prenner, *Biochim. Biophys. Acta*, 1999, **1462**, 14.
28 M. A. Yorek, in *Phospholipid Handbook*, ed. G. Cevc, Marcel Dekker, New York, 1993, p. 745.
29 L. D. Mayer, M. J. Hope, P. R. Cullis and A. S. Janoff, *Biochim. Biophys. Acta*, 1985, **817**, 193.
30 R. C. MacDonald, R. I. MacDonald, B. Ph, M. Menco, K. Takeshita, N. K. Subarrao and L. Hu, *Biochim. Biophys. Acta*, 1991, **1061**, 297.
31 M. C. Antunes-Madeira, R. A. Videira and V. M. C. Madeira, *Biochim. Biophys. Acta*, 1994, **1190**, 149.
32 T. Heimburg, *Biochim. Biophys. Acta*, 1998, **1415**, 147.
33 H. J. Hinz and J. M. Sturtevant, *J. Biol. Chem*., 1972, **247**, 6071.
34 O. G. Mouritsen and M. Bloom, *Biophys. J*., 1984, **46**, 141.
35 G. D. Hunter, *Biochem. J*., 1969, **114**, 22p.
36 L. Meda, M. Cassatella, G. I. Szendrei, L. Oltvos Jr, P. Baron, M. Villalba, D. Ferrari and F. Rossi, *Nature*, 1995, **374**, 647.
37 C. Selvaggini, L. De Gioia, L. Cantù, E. Ghibaudi, L. Diomede, O. Bugiani, G. Forloni, F. Tagliavini and M. Salmona, *Biochem. Biophys. Res. Commun*., 1993, **194**, 1380.
38 L. De Gioia, C. Selvaggini, E. Ghibaudi, L. Diomede, O. Bugiani, G. Forloni, F. Tagliavini and M. Salmona, *J. Biol. Chem*., 1994, **269**, 1.
39 O. Bugiani, L. Diomede, M. Algeri, L. De Gioia, T. Florio, G. Schettini, F. Tagliavini, G. Forloni and M. Salmona, *J. Neuropathol. Exp. Neurol*., 1995, **54**, 449.
40 A. J. Verkleij, R. F. Zwaal, B. Roelofsen, P. Comfurius, D. Kastelijn and L. V. Deenen, *Biochim. Biophys. Acta*, 1973, **323**, 178.
41 L. De Gioia, C. Selvaggini, E. Ghibaudi, L. Diomede, O. Bugiani, G. Forloni, F. Tagliavini and M. Salmona, *J. Biol. Chem*., 1994, **269**, 7859.